Polymer Chemistry

PAPER

View Article Online
View Journal

Cite this: DOI: 10.1039/c5py01537e

Unexpected fluorescence from maleimide-containing polyhedral oligomeric silsesquioxanes: nanoparticle and sequence distribution analyses of polystyrene-based alternating copolymers†

Mohamed Gamal Mohamed, Kuo-Chih Hsu, Jin-Long Hong and Shiao-Wei Kuo*

Received 22nd September 2015,
Accepted 19th October 2015

DOI: 10.1039/c5py01537e

www.rsc.org/polymers

In this study, we synthesized unusual fluorescent polyhedral oligomeric silsesquioxane (POSS)-containing polymers lacking any common fluorescent units (*e.g.*, phenyl or heterocyclic rings): a poly(maleimide isobutyl POSS) [poly(MIPOSS)] homopolymer and poly(styrene-*alt*-maleimide isobutyl POSS) [poly(S-*alt*-MIPOSS] and poly(4-acetoxystyrene-*alt*-maleimide isobutyl POSS) [poly(AS-*alt*-MIPOSS)] alternating copolymers, through free radical polymerization, and a poly(4-hydroxystyrene-*alt*-maleimide isobutyl POSS) [poly(HS-*alt*-MIPOSS)] alternating copolymer, through acetoxy hydrazinolysis of poly(AS-*alt*-MIPOSS). We used ^{1}H, ^{13}C, and ^{29}Si nuclear magnetic resonance spectroscopy, Fourier transform infrared (FTIR) spectroscopy, and MALDI-TOF mass spectrometry to examine the chemical structures and sequence distributions of these POSS-containing polymers. The FTIR spectra revealed the existence of specific intermolecular interactions, namely dipole–dipole interactions between the C=O groups in poly(MIPOSS) and poly(AS-*alt*-MIPOSS) and intermolecular hydrogen bonding between the C=O groups of the MIPOSS units and the OH groups of the HS units in poly(HS-*alt*-MIPOSS). Differential scanning calorimetry and thermogravimetric analyses revealed that the incorporation of MIPOSS units could enhance the thermal stability, but decrease the glass transition temperatures, of these alternating copolymers. The photoluminescence emission of poly(MIPOSS) was greater than those of the POSS-containing alternating copolymers, presumably because of the former's crystallinity and clustering of locked C=O groups of POSS units.

Introduction

Luminescent materials are attractive for academic research and have technical significance because of their possible application in drug delivery,[1] chemical sensors,[2] DNA probing,[3] protein sensors,[4] and cellular bioimaging.[5] The most luminescent materials are often quantum dots,[6] fluorescent organic dyes,[7] and fluorescent proteins.[8] Many fluorescent organic materials containing heterocyclic or benzene units exhibit aggregation-caused quenching (ACQ). Such ACQ luminescent materials are highly emissive in solution, but nonemissive in their aggregated or condensed states.[9–11] Tang *et al.* discovered, however, some small organic and polymeric fluorescent materials, based on silole derivatives, that display strong emissions when concentrated in solution or in the solid state; these materials are aggregation-induced emission (AIE) fluorescent materials.[12–14]

Most fluorescent polymeric materials feature π-aromatic units (benzene or heterocyclic rings) as emissive units.[15,16] Recently, fluorescent polymers lacking such conventional fluorescent units have attracted much attention for their excellent biocompatibility and biodegradability. For example, Tang *et al.* also found that polymerization of nonluminescent monomers – through free radical polymerization, reversible addition/fragmentation chain transfer (RAFT), or atom transfer radical polymerization – lacking luminescent groups can also give highly emissive polymeric materials.[15,16] In addition, Tang and coworkers observed that alternating poly(vinyl acetate-*alt*-maleic anhydride) nanoparticles exhibited strong light emission and AIE effects because of intermolecular interactions between their five membered dihydrofuran-2,5-dione groups or clustering of their locked C=O groups.[16] In addition, hyperbranched polymers featuring tertiary amino units, including polyureas,[17] poly(ether amide)s,[18] poly(amido amine)s,[19] and poly(amino ester)s,[20] can act as luminescent polymers. The emission mechanism of these materials originates from the

Department of Materials and Optoelectronic Science, Center for Nanoscience and Nanotechnology, National Sun Yat-Sen University, Kaohsiung, 804, Taiwan. E-mail: kuosw@faculty.nsysu.edu.tw

†Electronic supplementary information (ESI) available. See DOI: 10.1039/c5py01537e

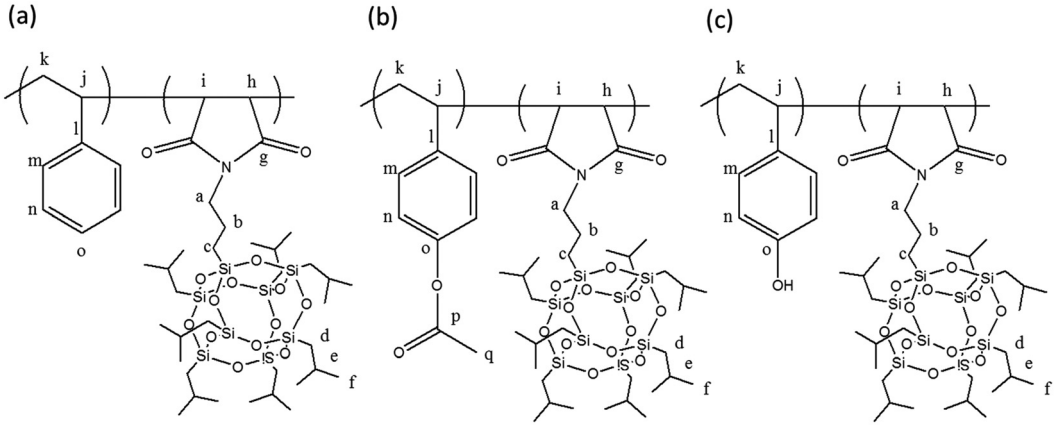

Scheme 1 Chemical structures and peak assignments for NMR spectra of poly(S-*alt*-MIPOSS), poly(AS-*alt*-MIPOSS) and poly(HS-*alt*-MIPOSS) copolymers.

presence of the tertiary amino moieties.[21,22] Succinimide derivatives are known fluorescence quenchers of proteins, and maleic anhydride-containing polymers can display fluorescence.[23] Polyisobutene succinic anhydrides and their imides have displayed unexpected emissions that have been attributed to the AIE effects of their C═O groups.[24]

Polyhedral oligomeric silsesquioxane (POSS) and its derivatives comprise an intriguing class of compounds that can be considered as nanostructured inorganic composites or organic/inorganic hybrid materials.[25–30] POSS derivatives have been studied in academic and industrial fields because of their interesting interfacial interactions; they have well-defined cubic three-dimensional cage-like structures with a chemical formula $(RSiO_{1.5})_8$, where the R unit is an organic group that can impart solubility and compatibility within a polymer matrix – indeed, the introduction of POSS moieties into polymer matrices can result in novel polymers displaying interesting mechanical properties, high thermal stabilities, and low flammability.[31–35] Hayakawa and Gopalan successfully synthesized the polystyrene-*b*-PMAPOSS (poly(methacrylate POSS) diblock copolymers with well-defined molecular distributions and high degrees of polymerization; these polymers exhibited microphase-separated structures.[36–38] Monticelli *et al.* grafted a titanium-containing POSS (M-POSS) to the maleic anhydride groups of a poly(styrene-*alt*-maleic anhydride) copolymer; the resulting nanofiber/M-POSS system displayed good photocatalytic activity for the degradation of sulforhodamine B, an organic dye.[39] Recently, Zhang *et al.* synthesized the alternating copolymer poly(styrene-*alt*-maleimide isobutyl POSS) [poly(S-*alt*-MIPOSS)] through RAFT polymerization, finding that incorporation of the MIPOSS moieties greatly enhanced the thermal properties of the copolymers.[40] Zhang *et al.* also demonstrated that poly[MIPOSS-*alt*-vinylbenzyl poly(ethylene glycol)] [poly(MIPOSS-*alt*-VBPEG)] could self-assemble in aqueous solution to form spherical structures.[41]

In this study, we synthesized a poly(MIPOSS) homopolymer and POSS-containing poly(S-*alt*-MIPOSS) and poly(AS-*alt*-MIPOSS) alternating copolymers through facile and ordinary free radical polymerizations in the presence of AIBN as the initiator in THF solution. We then prepared a poly(HS-*alt*-MIPOSS) alternating copolymer through acetoxy hydrazinolysis of poly(AS-*alt*-MIPOSS) using hydrazine monohydrate in 1,4-dioxane (Scheme 1). ^{1}H, ^{13}C, and ^{29}Si NMR spectroscopy, MALDI TOF mass spectrometry, and Fourier transform infrared (FTIR) spectroscopy confirmed their chemical structures. Furthermore, we employed differential scanning calorimetry (DSC) and thermogravimetric analysis (TGA) to determine the thermal degradation temperatures, char yields, and glass transition temperatures of the POSS-containing homopolymer and the alternating copolymers. FTIR spectra revealed the existence of specific intermolecular interaction, including dipole–dipole and hydrogen bonding interactions, in these POSS-containing polymers. We used wide-angle X-ray diffraction (WAXD) to examine the crystallinity of these POSS-containing polymers, and photoluminescence (PL) spectroscopy to study the optical properties of our POSS-containing alternating copolymers in solution and in the bulk state. To the best of our knowledge, we are the first to report the unusual fluorescent polyhedral oligomeric silsesquioxane (POSS)-containing polymers (poly(maleimide isobutyl POSS) lacking any common fluorescent unit by a simple free radical polymerization and study their emission behavior in the solid and solution states. In addition, we expect that these fluorescent alternating polymeric materials containing POSS nanoparticles can result in dramatic improvements in the physical properties such as a reduction in flammability and oxidation resistance.

Experimental section

Materials

Maleimide isobutyl POSS (MIPOSS) was purchased from Hybrid Plastics Company and used without purification. Methanol (MeOH), dichloromethane (DCM), tetrahydrofuran (THF), and hydrazine monohydrate ($N_2H_4{\cdot}H_2O$) were purchased from Alfa-Aesar. Azobisisobutyronitrile (AIBN) was

received from Sigma-Aldrich, recrystallized (MeOH) three times, and stored in a refrigerator to avoid decomposition. Styrene and 4-acetoxystyrene were purchased from Sigma-Aldrich; prior to polymerization, they were passed through an aluminum oxide column to remove any inhibitor and dried over CaH_2 for 24 h under a N_2 atmosphere. Polystyrene (molecular weight: 35 000 g mol^{-1}) was purchased from Sigma-Aldrich; poly(styrene-*alt*-maleic anhydride) (S-*alt*-MA) was synthesized according to a previous report.[16]

MIPOSS homopolymer through free radical polymerization

MIPOSS (3.00 g, 3.15 mmol) and AIBN (0.150 g) were dissolved in dry THF (30 mL) under a N_2 atmosphere in a 50 mL two-necked round-bottom flask equipped with a stirrer bar. The solution was carefully degassed through three freeze/thaw cycles to remove any O_2. The mixture was then heated at 70–80 °C for 24 h. The polymerization was quenched by cooling the flask in an ice bath and exposing the contents to air for 1 h. The crude polymer was precipitated from the reaction mixture into a large amount of cold MeOH. This crude polymer was then reprecipitated from cold THF/MeOH three times to remove any unreacted MIPOSS monomer and other byproducts. The resulting homopolymer was dried at 50 °C for 24 h under high vacuum to remove any residual solvents. ^{1}H NMR (500 MHz, $CDCl_3$, δ, ppm): 3.41 (polymer backbone and NCH_2CH_2), 1.85 [$CH(CH_3)_2$], 1.60 ($SiCH_2CH_2$), 0.96 [$CH(CH_3)_2$], 0.603 ($SiCH_2$). ^{13}C NMR (125 MHz, $CDCl_3$, δ, ppm): 177.58 (maleimide C=O), 41.62, 32.21, 29.34, 26.07, 25.73, 21.39, 9.45. FTIR (KBr, cm^{-1}): 1777 (asymmetric imide C=O stretching), 1709 (symmetric imide C=O stretching), 2946–2887 (isobutyl CH stretch), 1227 (CN bending vibration), and 1110 (Si–O–Si stretching of POSS core).

Poly(S-*alt*-MIPOSS) and poly(AS-*alt*-MIPOSS) alternating copolymers

MIPOSS (3.00 g, 3.15 mmol), styrene (0.328 g, 3.15 mmol) or 4-acetoxystyrene (0.511 g, 3.15 mmol), and AIBN (5 wt%) were dissolved in dry THF (50 mL) under a N_2 atmosphere in a 100 mL two-necked round-bottom flask equipped with a stirrer bar. The solution was carefully degassed through three freeze/thaw cycles to remove any O_2 and then heated at 70–80 °C for 24 h. The polymerization was quenched by cooling the flask in an ice bath and exposing the contents to air for 1 h. The crude polymer was obtained through precipitation of the reaction solution into a large amount of cold MeOH. The crude polymer was reprecipitated from cold THF/MeOH many times to remove any unreacted MIPOSS, styrene or acetoxystyrene, and other impurities. The resulting alternating copolymer was dried at 50 °C for 24 h under high vacuum to remove any residual solvent. For poly(S-*alt*-MIPOSS): ^{1}H NMR (500 MHz, $CDCl_3$, δ, ppm): 7.05 (ArH in polystyrene backbone), 3.41 (polymer backbone and NCH_2CH_2), 1.85 [$CH(CH_3)_2$], 1.60 ($SiCH_2CH_2$), 0.96 [$CH(CH_3)_2$], 0.60 ($SiCH_2$). ^{13}C NMR (125 MHz, $CDCl_3$, δ, ppm): 178.31 (maleimide C=O), 169.63, 151.21, 130.58, 122.64, 41.62, 30.07, 9.84. FTIR (KBr, cm^{-1}): 1772 (asymmetric C=O stretching, imide and C=O, $OCOCH_3$ group), 1705 (symmetric imide C=O stretching), 1227 (CN bending), 1110 (Si–O–Si stretching of POSS core). For poly(AS-*alt*-MIPOSS), most of the signals in the ^{1}H and ^{13}C NMR spectra were the same as those for poly(S-*alt*-MIPOSS), with the following exceptions: ^{1}H NMR, 2.27 ($OCOCH_3$); ^{13}C NMR, 179.07 (C=O imide), 170.05 (C=O acetate), 21.40 (CH_3).

Poly(HS-*alt*-MIPOSS) alternating copolymer

A solution of poly(AS-*alt*-MIPOSS) (2.00 g) in 1,4-dioxane (25 mL), in a 50 mL two-necked round-bottom flask equipped with a stirrer bar, was placed in an ice bath at 0 °C for 30 min under a N_2 atmosphere and then hydrazine monohydrate (15.5 g, 3.10 mmol) was added dropwise. The reaction mixture was then stirred overnight at room temperature. The organic phase was extracted into DCM (3 × 50 mL) to remove any excess hydrazine monohydrate. The combined organic phases were dried ($MgSO_4$) for 1 h and then removed the DCM solution by using a rotary evaporator to give a white powder. ^{1}H NMR (500 MHz, $CDCl_3$, δ, ppm): 7.05 (ArH in polystyrene backbone), 3.23 (polymer backbone and NCH_2CH_2), 1.83 [$CH(CH_3)_2$], 1.65 (NCH_2CH_2). ^{13}C NMR (125 MHz, $CDCl_3$, δ, ppm): 179.42 (maleimide C=O), 156.62, 130.58, 116.49, 41.62, 29.34, 9.84. FTIR (KBr, cm^{-1}): 3390 (OH stretching), 2946–2887 (isobutyl group), 1774 (asymmetric C=O, imide), 1704 (symmetric C=O stretching, imide), 1227 (CN bending), 1110 (Si–O–Si stretching of POSS core). Table 1 summarizes the properties of the poly(MIPOSS) homopolymer and these three alternating copolymers.

Table 1 The molecular weight, glass transition temperature and quantum yield of poly(MIPOSS), poly(S-*alt*-MIPOSS), poly(AS-*alt*-MIPOSS) and poly(HS-*alt*-MIPOSS)

Sample	M_n [a]	PDI[a]	M_n [b]	PDI[b]	T_g [c] (°C)	λ_{ab} [d] (nm)	Quantum yield[e] (%)
MIPOSS	2544.1	1.08	2110	1.33	—	237.3/280.0	72.5
S-*alt*-MIPOSS	3887.9	1.12	14 600	1.98	103	236.0/259.3	55.5
AS-*alt*-MIPOSS	2915.4	1.16	6570	1.64	75	235.7/262.5	46.8
HS-*alt*-MIPOSS	3155.9	1.16	5370	1.88	96	236.1/278.7	7.0

[a] Measured by MALDI-TOF MS analysis. [b] Measured by GPC. [c] Measured by DSC. [d] Determined by UV-vis absorption measurement. [e] Determined by using an integrated sphere by Ocean Optics.

Characterization

^{1}H and ^{13}C NMR spectra were recorded using an INOVA 500 with $CDCl_3$ as the solvent with tetramethylsilane (TMS) as an internal reference. FTIR spectra of polymer films were recorded using a Bruker Tensor 27 FTIR spectrophotometer; 32 scans were collected at a spectral resolution of 4 cm^{-1}. Mass spectra were recorded using a Bruker Daltonics Autoflex III MALDI-TOF mass spectrometer and the following voltage parameters: 19.06 and 16.61 kV for ion sources; 8.78 kV for lens; and 21.08 and 9.73 kV for reflectors. DSC measurements were performed using a TA Q-20 system, with N_2 as a purge gas (50 mL min^{-1}), and at a heating rate of 20 °C min^{-1}. The sample (*ca.* 3–5 mg) was placed in a sealed aluminum sample pan. The thermal stabilities of the homopolymer and alternating copolymers were investigated using a TA Q-50 thermogravimetric analyzer, with N_2 as a purge gas (60 mL min^{-1}), and at a heating rate of 20 °C min^{-1} from 30 to 800 °C. Molecular weights and molecular weight distributions (PDI) were determined through gel permeation chromatography (GPC) using a Waters 1515 HPLC equipped with refractive index detector and three ultrastragel columns. The GPC system was calibrated using polystyrene as the standard and THF was used as an eluent at a flow rate of 1 mL min^{-1}. UV-Vis spectra were recorded using a Shimadzu mini 1240 spectrophotometer; the concentration of polymers in THF was 10^{-4} M. PL spectra were collected at room temperature using a monochromatized Xe light source, solutions of polymers in THF at a concentration of 10^{-4} M, and an excitation wavelength of 330 nm. WAXD profiles were measured using the wiggler beamline BL17A1 of the National Synchrotron Radiation Research Center (NSRRC) of Taiwan. A triangular bent Si (111) single crystal was used to obtain a monochromated beam with a wavelength (λ) of 1.33 Å. The samples were annealed prior to WAXD measurements. The quantum efficiencies (Φ_f) of poly(MIPOSS), poly(S-*alt*-MIPOSS), poly(AS-*alt*-MIPOSS), poly(HS-*alt*-MIPOSS), and poly(S-*alt*-MA) in the solid state were measured on an integrated sphere (Ocean Optics). The quantum efficiencies (Φ_f) of poly(MIPOSS), poly(S-*alt*-MIPOSS), poly(AS-*alt*-MIPOSS), poly(HS-*alt*-MIPOSS), and poly(S-*alt*-MA) in the solution state were determined by using a quinine sulfate as the standard solution. The particle sizes of the shrunken aggregates of poly(MIPOSS) and poly(S-*alt*-MIPOSS) in THF/H_2O mixed media were evaluated by dynamic light scattering (DLS) using a Brookhaven 90 plus spectrometer equipped with a temperature controller.

Results and discussion

The incorporation of POSS into a polymer matrix can afford organic/inorganic hybrid materials displaying good thermal stability, oxidation resistance, and high mechanical properties.[26,40,41] In this study, we synthesized four new POSS-containing polymers: a poly(MIPOSS) homopolymer and poly(S-*alt*-MIPOSS) and poly(AS-*alt*-MIPOSS) alternating copolymers, prepared through a simple and convenient free radical polymerization using AIBN as the initiator, and a poly(HS-*alt*-MIPOSS) alternating copolymer, prepared through deacetylation of poly(AS-*alt*-MIPOSS) in 1,4-dioxane/hydrazine monohydrate at room temperature. We used ^{1}H, ^{13}C, and ^{29}Si NMR spectroscopy, FTIR spectroscopy, GPC (Fig. S1†) and MALDI-TOF mass spectrometry to confirm the molecular structures of these POSS-containing polymers. Fig. 1 displays the ^{1}H NMR spectra of poly(MIPOSS) and the alternating copolymers. The ^{1}H NMR spectrum of the poly(MIPOSS) homopolymer [Fig. 1(a)] features a signal at 3.45 ppm representing the main chain of the maleimide isobutyl POSS; a signal for the $SiCH_2CH_2CH_2N$ methylene protons at 3.45 ppm; signals at 1.82, 1.65, and 0.94 ppm for the $SiCH_2CH(CH_3)_2$ methine, $SiCH_2CH_2CH_2N$ methylene, and $SiCH_2CH(CH_3)_2$ methyl groups, respectively; and a signal at 0.57 ppm for both the $SiCH_2CH_2CH_2N$ and $SiCH_2CH(CH_3)_2$ methylene groups.[40,42] The ^{1}H NMR spectra of poly(S-*alt*-MIPOSS), poly(AS-*alt*-MIPOSS), and poly(HS-*alt*-MIPOSS) [Fig. 1(b)–(d), respectively] feature additional signals between 6.67 and 7.06 ppm representing the protons of their aromatic moieties. Moreover, the signal at 2.27 ppm (peak **q**) in the spectrum of poly(AS-*alt*-MIPOSS) [Fig. 1(c)], representing the protons of the acetyl groups ($OCOCH_3$), disappeared completely after hydrolysis to the OH groups of poly(HS-*alt*-MIPOSS) [Fig. 1(d)].[42] Scheme 1 summarizes the other peak assignments.

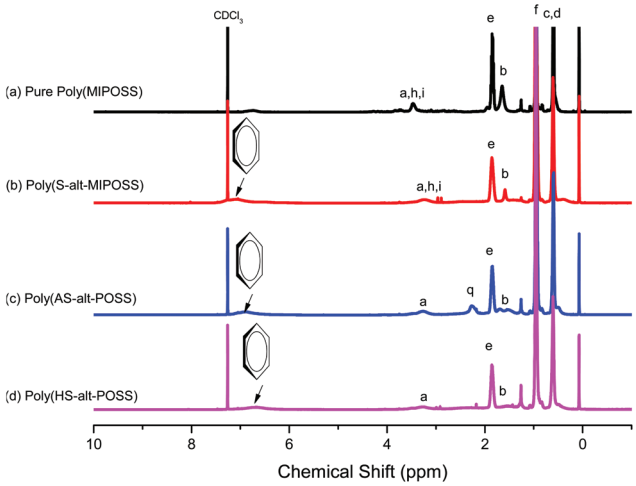

Fig. 1 ^{1}H NMR spectra of (a) poly(MIPOSS), (b) poly(S-*alt*-MIPOSS), (c) poly(AS-*alt*-MIPOSS), and (d) poly(HS-*alt*-MIPOSS) in $CDCl_3$.

Fig. 2 displays the ^{13}C NMR spectra of these four polymeric compounds. The ^{13}C NMR spectrum of poly(MIPOSS) in $CDCl_3$ at room temperature [Fig. 2(a)] features signals at 177.96, 41.28, and 9.45 ppm, representing the resonances of the carbon nuclei of the C=O groups, the $SiCH_2CH_2CH_2N$ methylene unit, and the $SiCH_2CH(CH_3)_2$ methine unit, respectively. The spectrum of poly(S-*alt*-MIPOSS) [Fig. 2(b)] features an additional signal centered at 129.15 ppm, representing the carbon nuclei of the aromatic units. The signals of poly(AS-*alt*-MIPOSS) [Fig. 2(c)] appear at 179.07, 170.05, 151.23–123.01,

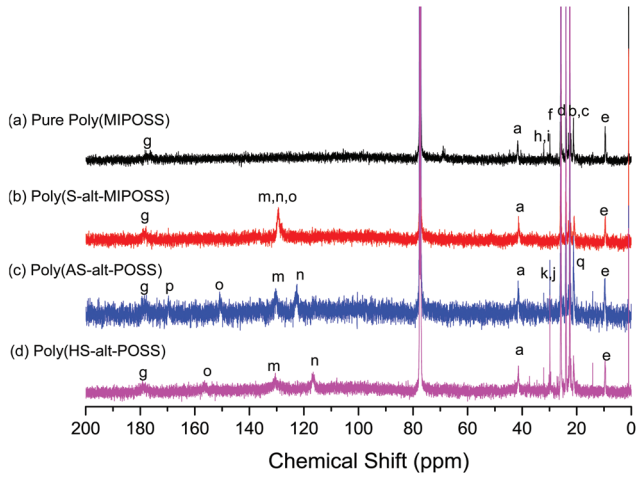

Fig. 2 ^{13}C NMR spectra of (a) poly(MIPOSS), (b) poly(S-*alt*-MIPOSS), (c) poly(AS-*alt*-MIPOSS), and (d) poly(HS-*alt*-MIPOSS) in $CDCl_3$.

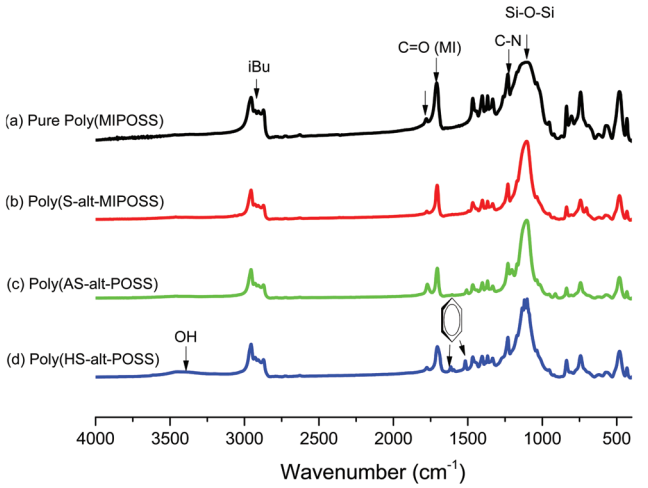

Fig. 4 FTIR spectra of (a) poly(MIPOSS), (b) poly(S-*alt*-MIPOSS), (c) poly(AS-*alt*-MIPOSS), and (d) poly(HS-*alt*-MIPOSS) at room temperature.

and 21.40 ppm, corresponding to the imide C═O, acetyl C═O, aromatic, and OCO**C**H$_3$ methyl groups, respectively. In Fig. 2(d), the absence of the signal (170.05 ppm) of the C═O group of the acetate units and the shifts of the signals of the carbon nuclei of the aromatic rings, to 156.09 (**Ph**OH, peak **o**) and 116.66 (peak **n**) ppm, confirmed the synthesis of poly(HS-*alt*-MIPOSS). Scheme 1 summarizes the other peak assignments. We could also use ^{13}C NMR spectroscopy to investigate the alternating copolymers of the maleimide isobutyl POSS and styrene derivatives; the signals of the quaternary carbon nuclei in the aromatic styrene units appear at 151.23–123.01 ppm, indicating that the sequence structures of the copolymers were non-alternating, semi-alternating, and alternating.[40,43,44] Fig. 3 presents the ^{29}Si NMR spectra of poly(MIPOSS), poly(S-*alt*-MIPOSS), poly(AS-*alt*-MIPOSS), and poly(HS-*alt*-MIPOSS) in $CDCl_3$. Two peaks appear, centered at −54.02 (peak **a**) and −54.44 ppm (peak **b**), corresponding to their O**Si**CH$_2$CH$_2$CH$_2$N and O**Si**CH$_2$CH(CH$_3$)$_2$ units, respectively. These ^{29}Si NMR spectra suggest that no cage cleavage occurred during the free radical polymerization, with the POSS cores remaining intact. Taken together, the NMR spectra are consistent with the chemical structures of the homopolymer and alternating copolymers.

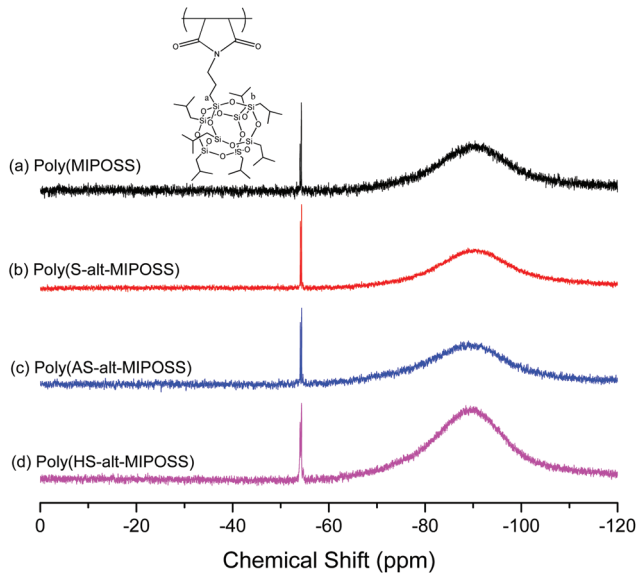

Fig. 3 ^{29}Si NMR spectra of (a) poly(MIPOSS), (b) poly(S-*alt*-MIPOSS), (c) poly(AS-*alt*-MIPOSS), and (d) poly(HS-*alt*-MIPOSS) in $CDCl_3$.

Fig. 4 displays the FTIR spectra of poly(MIPOSS), poly(S-*alt*-MIPOSS), poly(AS-*alt*-MIPOSS), and poly(HS-*alt*-MIPOSS) at room temperature. Characteristic absorption bands of the homopolymer and alternating copolymers appear at 2952–2874, 1781, 1709, and 1110 cm^{-1}, representing isobutyl CH stretching, asymmetric imide C═O stretching, symmetric imide C═O stretching, and Si–O–Si stretching in the maleimide isobutyl POSS structure. The spectrum of poly(HS-*alt*-MIPOSS) [Fig. 4(d)] features an absorption band at 3453 cm^{-1} for OH stretching; the signal at 1771 cm^{-1} for C═O stretching of the AS groups in Fig. 4(c) only decreased after deacetylation because it overlapped with the signal for asymmetric imide C═O stretching.

Fig. 5 displays FTIR spectra, in the range 1850–1650 cm^{-1}, that reveal the presence of specific interactions in the alternating polymers. The spectrum of poly(MIPOSS) [Fig. 5(a)] features two characteristic absorption bands centered at 1781 and 1709 cm^{-1}, corresponding to asymmetric imide C═O and symmetric imide C═O stretching, respectively. These absorption bands shifted to lower frequencies for poly(S-*alt*-MIPOSS) [to 1774 and 1706 cm^{-1}, respectively; Fig. 5(b)] and poly(AS-*alt*-MIPOSS) [to 1771 and 1705 cm^{-1}, respectively; Fig. 5(c)]. More interestingly, the width at half-height decreased from 32.3 cm^{-1} for poly(MIPOSS) to 19.8 and 20.2 cm^{-1} for poly(S-*alt*-MIPOSS) and poly(AS-*alt*-MIPOSS), respectively, implying

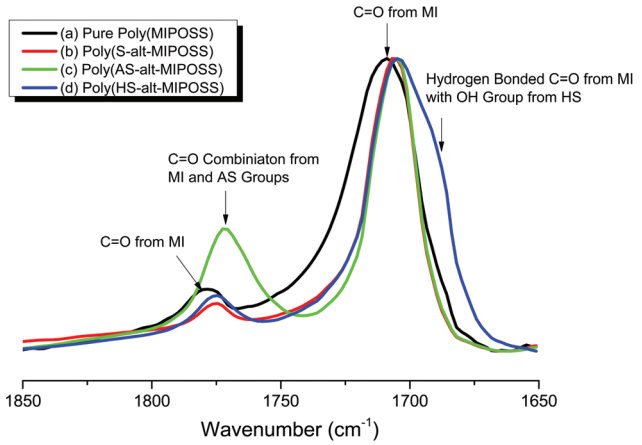

Fig. 5 FTIR spectra, in the range 1850–1650 cm^{-1}, of (a) poly(MIPOSS), (b) poly(S-*alt*-MIPOSS), (c) poly(AS-*alt*-MIPOSS), and (d) poly(HS-*alt*-MIPOSS), recorded at room temperature.

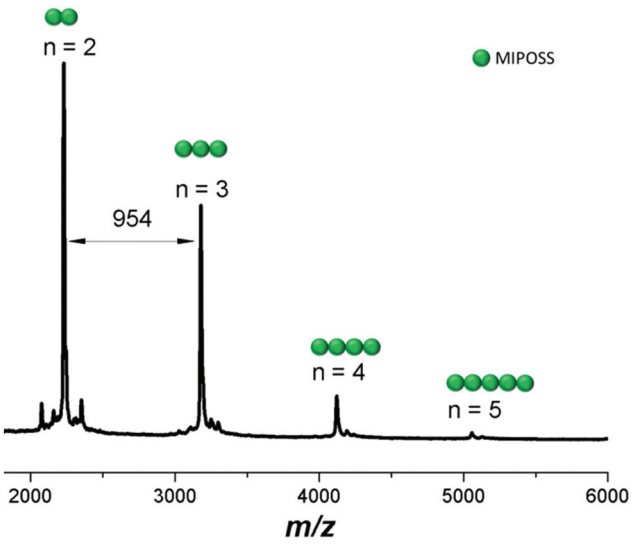

Fig. 6 MALDI-TOF mass spectrum of poly(MIPOSS).

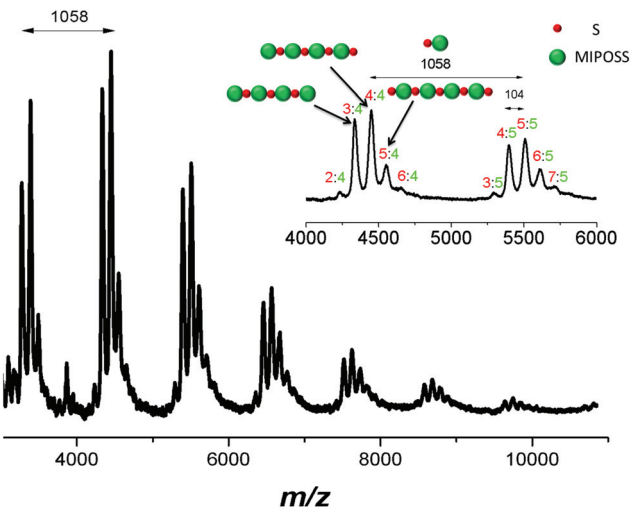

Fig. 7 MALDI-TOF mass spectrum of poly(S-*alt*-MIPOSS).

that the dipole–dipole interactions between the imide C═O groups of poly(MIPOSS) were disrupted and weakened upon insertion of the styrene and acetoxystyrene segments. The FTIR spectrum of poly(HS-*alt*-MIPOSS) [Fig. 4(d)] reveals that the signals of the C═O groups shifted to 1774 and 1704 cm^{-1}, respectively, with a new signal appearing at 1688 cm^{-1}, suggesting that hydrogen bonds existed between the C═O groups of the MIPOSS units and the phenolic OH groups of the HS units.[45] Through curve-fitting with the Gaussian function, we calculated the area fraction of the hydrogen-bonded C═O groups of the MIPOSS units to be 39.3%.

We recorded MALDI-TOF mass spectra to determine the molecular weights of our POSS-containing polymers and the sequence distributions of our alternating copolymers. It can be difficult to measure MALDI-TOF profiles of high-molecular-weight compounds because the mass resolution can be too weak to separate the individual chains.[46–48] Fig. 6 displays the MALDI-TOF mass spectrum of poly(MIPOSS), revealing that the molar mass of its individual chains could be determined. For example, the intense peaks *m*/*z* 2230.80, 3184.95, 4124.30, and 5065.17 correspond to two, three, four, and five units, respectively, of maleimide isobutyl POSS. The difference in the values of *m*/*z* between 2230.95 and 3184.30 is 954, equal to the molecular weight of the repeat unit of poly(MIPOSS). The difference in the values of *m*/*z* between 3184.95 and 4124.30 is not, however, equal to 954, probably because of the different chain ends after thermal fragmentation of AIBN after free radical polymerization.

Fig. 7 presents the mass spectrum of poly(S-*alt*-MIPOSS), where the intensities of the individual peaks are not exactly 100%, providing excellent evidence for its copolymer composition: perfectly alternating individual chains with equal numbers of styrene and MIPOSS units. By using MIPOSS as a monomer for free radical copolymerization, it became easy to distinguish the sequence distribution in the MALDI-TOF mass spectrum; because the molecular weight of MIPOSS is quite high (954 g mol^{-1}), we could readily determine the number of units of MIPOSS in the poly(S-*alt*-MIPOSS) alternating copolymer. For example, the peak at *m*/*z* 4448.72 corresponds to four units of styrene and four units of MIPOSS, while that at *m*/*z* 5506.79 corresponds to five units of styrene and five units of MIPOSS, indicating that poly(S-*alt*-MIPOSS) had a perfectly alternating sequence of individual chains. The difference in the values of *m*/*z* between 4448.72 and 5506.79 is 1058 g mol^{-1}, equal to the molecular weight of one styrene and one MIPOSS unit. The intense peak at *m*/*z* 4448.72 corresponds to four units of styrene (4 × 104.15 u), four units of MIPOSS (4 × 954 u), a chain end from AIBN, and a Ag ion (107.87 u); it is labeled 4 : 4. The most intense peaks correspond to a perfectly alternating sequence, with ratios of styrene : MIPOSS of $n-1:n$, $n:n$, and $n+1:n$, such as 3 : 4, 4 : 4, and 5 : 4 (see the

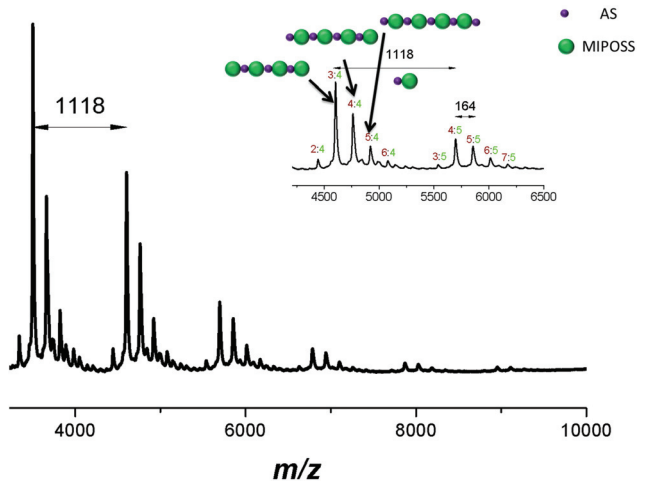

Fig. 8 MALDI-TOF mass spectrum of poly(AS-*alt*-MIPOSS).

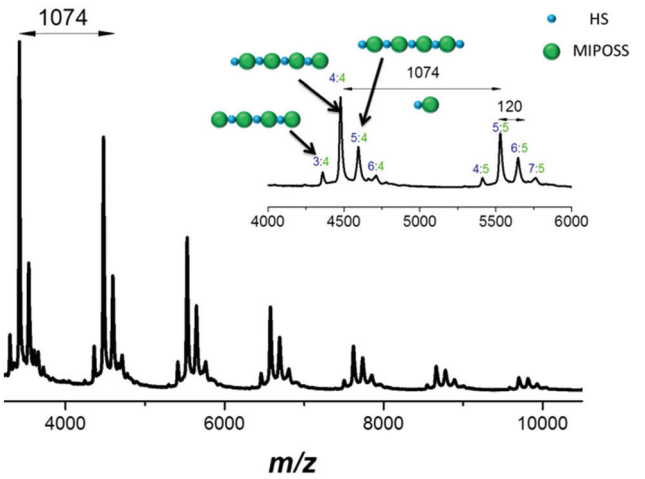

Fig. 9 MALDI-TOF mass spectrum of poly(HS-*alt*-MIPOSS).

inset to Fig. 7). Only a few weak peaks correspond to the ratios of styrene : MIPOSS of $n - 2 : n$ and $n + 2 : n$, such as 2 : 4 and 6 : 4, arising due to homopolymerization of styrene and MIPOSS; the fraction of such non-alternating segments was only 3.9%, based on the results of curve-fitting. Thus, MALDI-TOF mass spectral analysis suggested that we had obtained a near-perfect alternating copolymer of poly(S-*alt*-MIPOSS).

Interestingly, the mass spectrum of poly(AS-*alt*-MIPOSS) (Fig. 8) exhibited the same phenomenon as that of poly(S-*alt*-MIPOSS); for example, an intense peak at *m*/*z* 4761.6 (labeled 4 : 4) corresponding to four units of 4-acetoxystyrene (4 × 162.19 u), four units of MIPOSS (4 × 954 u), a chain end from AIBN, and a Ag ion (107.87 u), as well as a peak at *m*/*z* 5879.3 (labeled 5 : 5) representing five units of MIPOSS and five units of 4-acetoxystyrene. The difference in the values of *m*/*z* between 4761.6 and 5879.3 is 1118 g mol^{-1}, equal to the molecular weight of one 4-acetoxystyrene unit and one MIPOSS unit. Similarly, only a few weak peaks appeared corresponding to ratios of 4-acetoxystyrene : MIPOSS of $n - 2 : n$ and $n + 2 : n$, such as 2 : 4 and 6 : 4, arising from homopolymerization of 4-acetoxystyrene and MIPOSS units, with the fraction of non-alternating segments being only 2.7% based on curve-fitting. This MALDI-TOF mass spectral analysis also implies that we had obtained a near-perfect alternating copolymer of poly(AS-*alt*-MIPOSS). The MALDI-TOF mass spectrum in Fig. 9 confirms that the chain of poly(HS-*alt*-MIPOSS) was also an alternating copolymer, with the intense peak at *m*/*z* 4478.6 (labeled 4 : 4) representing four units of 4-hydroxystyrene (4 × 120 u), four units of MIPOSS (4 × 954 u), a chain end from AIBN, and a Ag ion (107.87 u), as well as a signal at *m*/*z* 5552.3 (labeled 5 : 5) attributable to five units of MIPOSS and five units of 4-hydroxystyrene. The difference in the values of *m*/*z* between 4478.6 and 5552.3 is 1074 g mol^{-1}, equal to the molecular weight of one 4-hydroxystyrene unit and one MIPOSS unit. The sequence distribution of poly(HS-*alt*-MIPOSS) should be the same as that of poly(AS-*alt*-MIPOSS), because we prepared it through deacetylation of the latter. Based on their MALDI-TOF mass spectra, our three copolymers appeared to be near-perfect alternating copolymers.

Thermal properties of homopolymer and alternating copolymers

To elucidate the thermal properties of the homopolymer and alternating copolymers, we subjected them all to DSC and TGA under a N_2 atmosphere. Fig. 10 presents the DSC profiles of poly(MIPOSS), poly(S-*alt*-MIPOSS), poly(AS-*alt*-MIPOSS), and poly(HS-*alt*-MIPOSS). The DSC trace of poly(MIPOSS) [Fig. 10(a)] features an endothermic melting point at 154 °C and an exothermic crystalline peak at 70 °C (data not shown), suggesting that poly(MIPOSS) possessed a crystalline structure because of POSS aggregation. The introduction of POSS into a polymer can increase the glass transition temperature (T_g) of

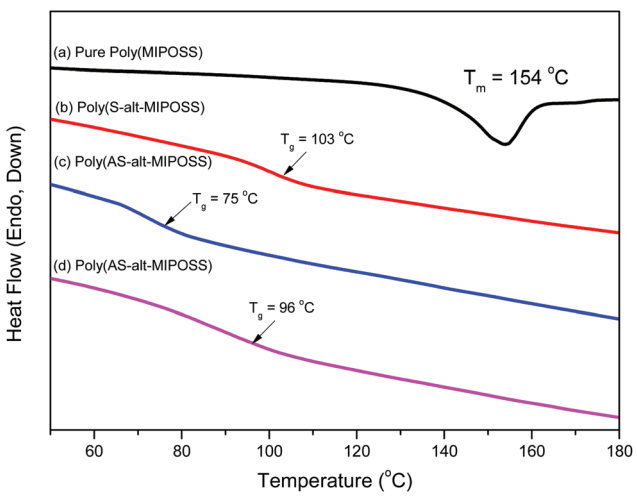

Fig. 10 DSC thermograms of (a) poly(MIPOSS), (b) poly(S-*alt*-MIPOSS), (c) poly(AS-*alt*-MIPOSS), and (d) poly(HS-*alt*-MIPOSS).

the resulting organic/inorganic hybrid material because of the rigid structure of the POSS cages and the restricted movement of the polymer chains.[40,42] The glass transition temperature (103 °C) of poly(S-*alt*-MIPOSS) [Fig. 10(b)] was higher than that of PS at a similar molecular weight (T_g = 90 °C; 5000 g mol^{-1}), presumably because of the rigid cage structure of the MIPOSS units. An unusual and interesting phenomenon is evident in Fig. 10(c) and (d). The value of T_g of poly(AS-*alt*-MIPOSS) decreased to 75 °C while that of poly(HS-*alt*-MIPOSS) increased to 96 °C after deacetylation, due to hydrogen bonding between the OH groups of the HS units and the C=O groups of the MIPOSS units.[45] Nevertheless, the values of T_g of the poly(AS-*alt*-MIPOSS) and poly(HS-*alt*-MIPOSS) alternating copolymers were significantly lower than those of PAS (T_g = 122 °C) and PHS (T_g = 150 °C) of similar molecular weights, and even lower than that of poly(S-*alt*-MIPOSS) lacking the AcO and OH functional groups. The glass transition temperature of PAS is higher than that of PS because the functional AcO groups of PAS enhance the intermolecular dipole–dipole interactions among the C=O groups of the PAS segments; after deacetylation to form PHS, the glass transition temperature would increase further because of intermolecular hydrogen bonding among the OH groups of the PHS segments. A possible reason for the low value of T_g of poly(AS-*alt*-MIPOSS) is that the self-association dipole–dipole interactions of its AS···AS or MIPOSS···MIPOSS segments were disrupted significantly after inserting the AS units alternatively into the MIPOSS units. This hypothesis is consistent with the significant decrease in the widths at half-height, from 32.3 cm^{-1} for poly(MIPOSS) to 20.2 cm^{-1} for poly(AS-*alt*-MIPOSS), in the FTIR spectra. Scheme 1 and Fig. 8 reveal that the alternative insertion of bulky MIPOSS units into PAS segments strongly hindered the self-association dipole–dipole interactions (inter- or intra-chain) among the PAS segments; thus, the bulky POSS units provided a strong screening effect that decreased the possibility of intermolecular interaction, thereby lowering the value of T_g. A similar reason might also explain the lower value of T_g of poly(HS-*alt*-MIPOSS): the inter- and intra-chain hydrogen bonding of the self-associating OH···OH groups of PHS would decrease significantly as a result of the strong intramolecular screening effect of bulky MIPOSS units. Such OH groups from the HS units would be able to interact only with the C=O groups of the MIPOSS units through weaker intra-chain OH···O=C hydrogen bonding. Therefore, the broad band at 3350 cm^{-1} representing a strong self-association of the OH···OH units of PHS shifted to a higher wavenumber of 3453 cm^{-1} for the weaker inter-association of OH···O=C groups; correspondingly, the value of T_g decreased because no strong intermolecular hydrogen bonding interactions could occur among the PHS segments.

We recorded WAXD patterns (Fig. 11) of poly(MIPOSS), poly(S-*alt*-MIPSS), poly(AS-*alt*-MIPOSS), and poly(HS-*alt*-MIPOSS) at room temperature to examine their crystallinity. The WAXD profile of poly(MIPOSS) features four major diffraction peaks at 7.06 (101), 9.50 (110), 10.60 (102), and 16.43 (113) corresponding to the rhombohedral crystal structure of MIPOSS;[49,50]

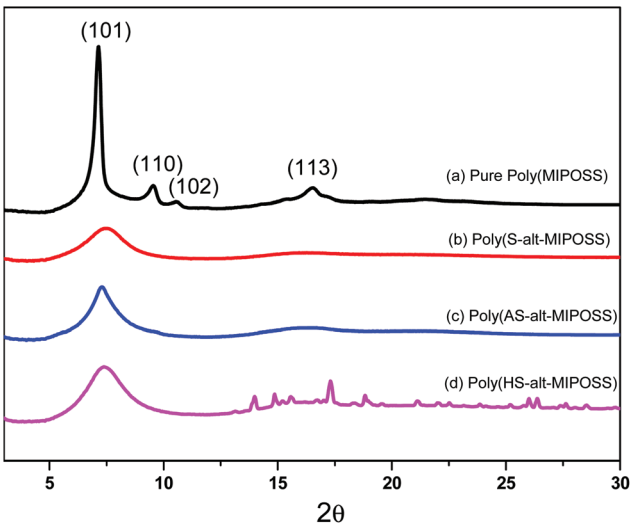

Fig. 11 Wide-angle X-ray diffraction (WAXD) patterns of (a) poly(MIPOSS), (b) poly(S-*alt*-MIPOSS), (c) poly(AS-*alt*-MIPOSS) and (d) poly(HS-*alt*-MIPOSS) alternating copolymers.

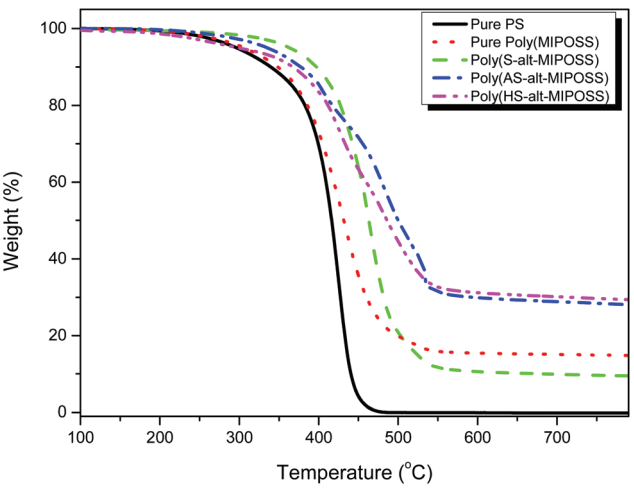

Fig. 12 TGA profiles of PS, poly(MIPOSS), poly(S-*alt*-MIPOSS), poly(AS-*alt*-MIPOSS), and poly(HS-*alt*-MIPOSS), recorded under a N_2 atmosphere.

accordingly, we observed a melting temperature, through DSC analyses, in Fig. 10. After alternative insertion of S, AS, and HS inert diluent segments into the MIPOSS segment, the WAXD patterns of poly(S-*alt*-MIPSS), poly(AS-*alt*-MIPOSS), and poly(HS-*alt*-MIPOSS) featured only broad peaks, with the crystalline peaks of poly(MIPOSS) disappearing; thus, these alternating copolymers had amorphous structures, consistent with DSC analyses in Fig. 10.

We performed TGA analyses under a N_2 atmosphere (Fig. 12) to determine the decomposition temperatures (T_{d10} as the standard) and char yields of these alternating copolymers prepared through free radical copolymerization. The

degradation temperature and char yield of poly(MIPOSS) (345 °C and 14.8%, respectively) were higher than those of PS (337 °C and 0%, respectively), consistent with the readier pyrolysis of the PS main chain from 300 to 450 °C.[51,52] More interestingly, the value of T_{d10} and the char yield of poly(S-*alt*-MIPOSS) (397 °C and 9.5%, respectively) were higher than those of the standard PS as a result of the steric bulk of the rigid-cage MIPOSS units. In contrast, both the poly(AS-*alt*-MIPOSS) (376 °C and 28.1%, respectively) and poly(HS-*alt*-MIPOSS) (366 °C and 29.3%, respectively) alternating copolymers displayed relatively lower degradation temperatures and relatively higher char yields than those of poly(S-*alt*-MIPOSS) because, above their decomposition temperature, their acetyl and phenol moieties would tend to form aromatic char structures and increase the crosslinking densities of their organic/inorganic copolymers.[50a]

Optical properties of poly(MIPOSS), poly(S-*alt*-MIPOSS), poly(AS-*alt*-MIPOSS), and poly(HS-*alt*-MIPOSS)

Poly(MIPOSS), poly(S-*alt*-MIPOSS), poly(AS-*alt*-MIPOSS), poly(HS-*alt*-MIPOSS) and poly(S-*alt*-MA) are soluble in THF, $CHCl_3$, DCM and DMF solutions. The UV-Vis absorption spectra of poly(MIPOSS) and other alternating copolymers in THF solution are shown in Fig. S2.† Poly(MIPOSS) and other alternating copolymers showed two major absorption peaks which can be assigned to the π–π* and n–π* transitions. The values of two major absorption peaks are summarized in Table 1.

We used PL spectroscopy to investigate the emission properties of the homopolymer and the alternating copolymers in the solid state and the fluorescence behavior of poly(MIPOSS) and poly(S-*alt*-MIPOSS) at various concentrations (from 10^{-5} to 10^{-2} M) in THF with excitation at 330 nm. Fig. 13 presents the PL spectra of poly(MIPOSS), poly(S-*alt*-MIPOSS), poly(AS-*alt*-MIPOSS), and poly(HS-*alt*-MIPOSS) in the solid state. The intensities of the unexpected emissions of the oxygenic non-conjugated poly(MIPOSS) at 490 and 519 nm were higher than those of the alternating copolymers, presumably because of the clustering of the locked C═O groups.[15,16] On the other hand, poly(S-*alt*-MIPOSS), poly(AS-*alt*-MIPOSS), and poly(HS-*alt*-MIPOSS) exhibited fluorescence that resulted from pi–pi interactions between the phenyl rings and C═O groups in poly(MIPOSS). In addition, the emission intensities of the copolymers were lower than those of poly(MIPOSS), suggesting a lower degree of clustering of the locked C═O units of poly(MIPOSS) after alternative insertion of the styrene derivatives. Fig. S3† displays the photoluminescence spectra of poly(MIPOSS), poly(S-*alt*-MIPOSS), poly(AS-*alt*-MIPOSS), poly(HS-*alt*-MIPOSS) and poly(S-*alt*-MA) in THF solution (10^{-3} M). As shown in Fig. S3,† poly(MIPOSS) shows a strong emission peak at 496 nm, referring to its bulky anhydride group in the maleimide isobutyl unit, which hinders the free rotation of polymer chains along the C–C single bond.[16b] Fig. 14 displays the effect of concentration on the emission behavior of poly(MIPOSS) and poly(S-*alt*-MIPOSS) in THF. The emission intensities of both poly(MIPOSS) and poly(S-*alt*-MIPOSS) increased upon increasing the concentration (from 10^{-5} to 10^{-2} M) in THF. In the most dilute solutions (10^{-5} M) of these oxygenic nonconjugated polymers, we observed no emissions because only a small amount of the luminogen was present.[9c,12b,16,53,54] To examine the aggregation induced emission behavior of poly(MIPOSS) and poly(S-*alt*-MIPOSS), the effects of water content on photoluminescence spectra were determined in a THF/water mixture as predicted in Fig. S4.† Water is used here because it is a poor solvent for poly(MIPOSS) and poly(S-*alt*-MIPOSS), respectively. On increasing the water content from 0 to 80%, the corresponding solution in solution mixtures exhibited increased emission intensity due to the aggregation of luminogenic molecules with high water contents. The for-

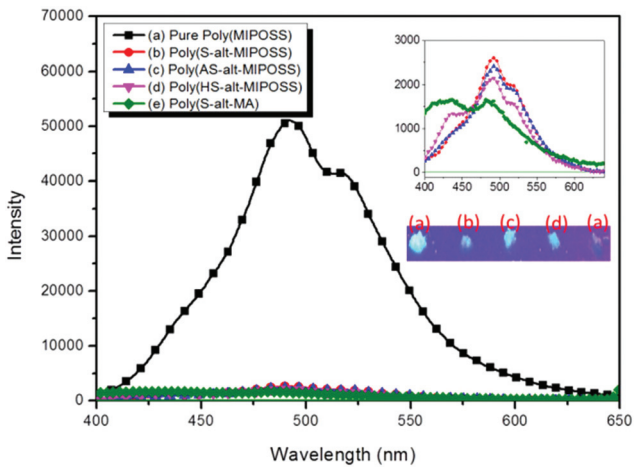

Fig. 13 PL spectra of (a) poly(MIPOSS), (b) poly(S-*alt*-MIPOSS), (c) poly(AS-*alt*-MIPOSS), (d) poly(HS-*alt*-MIPOSS), and (e) poly(S-*alt*-MA) in the solid state recorded with excitation at 330 nm. Photographs of poly(MIPOSS) and alternating copolymers in the solid state under 365 nm UV illumination.

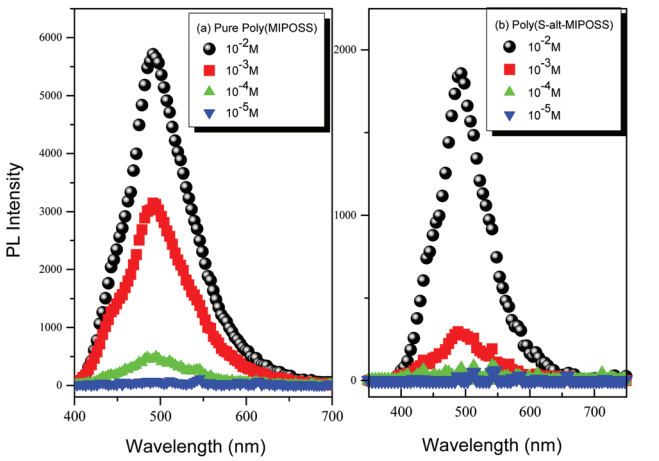

Fig. 14 Fluorescence spectra of (a) poly(MIPOSS) and (b) poly(S-*alt*-MIPOSS) as solutions in THF at concentrations from 10^{-5} to 10^{-2} M (excitation at 330 nm).

mation of a nanoaggregate structure has the role to activate the restriction of the intramolecular rotation (RIR) process. According to the concentration-enhanced emissions and the solvent pair effect in Fig. 14(A) and (B) and S4,† we suspect that poly(MIPOSS) and poly(S-*alt*-MIPOSS) may both be AIE materials. To confirm our hypothesis, we measured the quantum efficiencies (Φ_f) of poly(MIPOSS), poly(S-*alt*-MIPOSS), poly(AS-*alt*-MIPOSS), poly(HS-*alt*-MIPOSS), and poly(S-*alt*-MA) in the solid state, obtaining values of 72.5, 55.5, 46.8, 7.0, and 6.9%, respectively. Interestingly, the quantum efficiency of poly(S-*alt*-MIPOSS) was higher than that of poly(S-*alt*-MA), presumably because the POSS units were able to lock the C=O groups in the MIPOSS segments and, thereby, enhance the emission properties. In addition, the values of quantum efficiencies (Φ_f) of poly(MIPOSS), poly(S-*alt*-MIPOSS), poly(AS-*alt*-MIPOSS), poly(HS-*alt*-MIPOSS), and poly(S-*alt*-MA) in THF solution were 57.82, 5.52, 2.70, 5.64 and 1.72%, respectively. Dynamic light scattering (DLS) was measured to determine whether poly(MIPOSS) and poly(S-*alt*-MIPOSS) can form nanoaggregate structures in THF/H_2O mixture solution as shown in Fig. S5.† The sizes of the particles of poly(MIPOSS) were 733, 580, 383, and 225 nm. While the sizes of particles of poly(S-*alt*-MIPOSS) were 906, 774, 728 and 586 nm on increasing the water content from 40 to 80% in the THF/water mixture media. The formation of shrunken aggregates of poly(MIPOSS) and poly(S-*alt*-MIPOSS) in solution on increasing the water volume fraction is responsible for the emission intensity enhancement in Fig. S4.†

Conclusions

We have synthesized a poly(MIPOSS) homopolymer and poly(S-*alt*-MIPOSS), poly(AS-*alt*-MIPOSS), and poly(HS-*alt*-MIPOSS) alternating copolymers through facile free radical polymerizations, and characterized their chemical structures using NMR spectroscopy, FTIR spectroscopy, and MALDI-TOF mass spectrometry. TGA revealed that the thermal degradation temperatures and char yields of the POSS-containing alternating copolymers were improved after the incorporation of the MIPOSS units. Interestingly, WXRD analysis indicated that poly(MIPOSS) was a crystalline polymer, whereas the POSS-containing alternating polymers, formed after alternating insertion of styrene derivatives, were amorphous polymers. In addition, the emission of the oxygenic nonconjugated poly(MIPOSS) was stronger in the bulk state and its quantum efficiency was higher than those of the POSS-containing alternating copolymers; the emission of poly(MIPOSS) was associated with the molecular interactions between the five-membered dihydrofuran-2,5-dione rings and its highly crystallinity, as determined using PL spectroscopy and WXRD. A further study of the fluorescence mechanism of these POSS-containing alternating polymers might lead to the design of novel luminescent polymeric materials with various potential applications.

Acknowledgements

This study was supported financially by the Ministry of Science and Technology, Taiwan, Republic of China, under contracts MOST103-2221-E-110-079-MY3 and MOST102-2221-E-110-008-MY3.

References

1 (*a*) W. Zhang, L. Xu, J. Qin and C. Yang, *Macromol. Rapid Commun.*, 2013, **34**, 442–446; (*b*) D. D. Li, J. H. Yu and R. R. Xu, *Chem. Commun.*, 2011, **47**, 11077–11079; (*c*) Z. Song, Y. Hong, R. T. K. Kwok, J. W. Y. Lam, B. Liu and B. Z. Tang, *J. Mater. Chem. B*, 2014, **2**, 1717–1723.

2 (*a*) L. Prodi, F. Bolletta, M. Montali and N. Zaccheroni, *Coord. Chem. Rev.*, 2000, **205**, 59–83; (*b*) B. Wang and M. R. Wasielewski, *J. Am. Chem. Soc.*, 1997, **119**, 12–21.

3 K. Dore, S. Dubus, H. A. Ho, I. Levesque, M. Bruntte, G. Corbeil, M. Boissinot, G. Boivin, M. G. Bergeron, D. Boudreau and M. Leclerc, *J. Am. Chem. Soc.*, 2004, **126**, 4240–4244.

4 A. Keppler, H. Pick, C. Arrivoli, H. Vogel and K. Johnsson, *Proc. Natl. Acad. Sci. U. S. A.*, 2004, **101**, 9955–9959.

5 (*a*) D. D. Li, C. L. Miao, X. D. Wang, X. H. Yu, J. H. Yu and R. R. Xu, *Chem. Commun.*, 2013, **49**, 9549–9551; (*b*) Y. X. Wu, J. B. Li, L. H. Liang, D. Q. Lu, L. Zhang, G. J. Mao, L. Y. Zhou, X. B. Zhang, W. Tan, G. L. Shen and R. Q. Yu, *Chem. Commun.*, 2014, **50**, 2040–2042.

6 (*a*) Y. Song, S. Zhu and B. Yang, *RSC Adv.*, 2014, **4**, 27184–272000; (*b*) A. P. Alivistos, *Science*, 1996, **271**, 933–937.

7 M. Li, L. H. Feng, H. Y. Lu, S. Wang and C. F. Chen, *Adv. Funct. Mater.*, 2014, **24**, 4405–4412.

8 (*a*) D. C. Chudakov, M. V. Matz, S. Lukyanov and K. A. Lukyanov, *Physiol. Rev.*, 2010, **90**, 1103–1163; (*b*) J. N. Brantely, C. B. Bailey, J. R. Cannon, K. A. Clark, D. A. V. Bout, J. S. Brodbelt, A. T. K. Clay and C. W. Bielawski, *Angew. Chem., Int. Ed.*, 2014, **53**, 5088–5092.

9 (*a*) J. H. Wu and G. S. Liou, *Polym. Chem.*, 2015, **6**, 5225–5232; (*b*) B. P. Jiang, D. S. Guo, Y. C. Liu, K. P. Wang and Y. Liu, *ACS Nano*, 2014, **8**, 1609–1618; (*c*) L. Liu, B. Wu, P. Yu, R. X. Zhuo and S. W. Huang, *Polym. Chem.*, 2015, **6**, 5185–5189; (*d*) S. H. Huang, Y. W. Chaing and J. L. Hong, *Polym. Chem.*, 2015, **6**, 497–508.

10 (*a*) C. Munkholm, D. R. Parkinson and D. R. Walt, *J. Am. Chem. Soc.*, 1990, **112**, 2608–2612; (*b*) W. Dong, T. Fei, A. P. Cando and U. Scherf, *Polym. Chem.*, 2014, **5**, 4048–4053.

11 (*a*) M. Belletete, J. Bouchard, M. Leclerc and G. Durocher, *Macromolecules*, 2005, **38**, 880–887; (*b*) R. Jakubiak, C. J. Collison, W. C. Wan and L. Rothberg, *J. Phys. Chem. A*, 1999, **103**, 2394–2401.

12 (*a*) A. Qin, J. W. Y. Lam and B. Z. Tang, *Prog. Polym. Sci.*, 2012, **37**, 182–209; (*b*) Y. Gong, L. Zhao, Q. Peng, D. Fan, W. Z. Yuan, Y. Zhang and B. Z. Tang, *Chem. Sci.*, 2015, **6**, 4438–4444.

13 (*a*) L. Li, M. Chen, H. Zhang, H. Nie, J. Z. Sun, A. Qin and B. Z. Tang, *Chem. Commun.*, 2015, **51**, 4830–4833; (*b*) Y. Hong, J. W. Y. Lam and B. Z. Tang, *Chem. Soc. Rev.*, 2011, **40**, 5361–5388; (*c*) S. Bao, Q. Wu, W. Qin, Q. Yu, J. Wang, G. Liang and B. Z. Tang, *Polym. Chem.*, 2015, **6**, 3537–3542.

14 (*a*) X. Lou, Z. Zhao, Y. Hong, C. Dong, X. Min, Y. Zhuang, X. Xu, Y. Jia, F. Xia and B. Z. Tang, *Nanoscale*, 2014, **6**, 14691–14696; (*b*) N. Zhao, M. Li, Y. Yan, J. W. Y. Lam, Y. L. Zhang, Y. S. Zhao, K. S. Wong and B. Z. Tang, *J. Mater. Chem. C*, 2013, **1**, 4640–4646; (*c*) J. Chen, Z. Xie, J. W. Y. Lam, C. C. W. Law and B. Z. Tang, *Macromolecules*, 2003, **36**, 1108–1117; (*d*) J. Chen, C. C. W. Law, J. W. Y. Lam, Y. Dong, S. M. F. Lo, I. D. Williams, D. Zhu and B. Z. Tang, *Chem. Mater.*, 2003, **15**, 1535–1546.

15 T. Huang, Z. Wang, A. Qin, J. Z. Sun and B. Z. Tang, *Acta Chim. Sin.*, 2013, **71**, 973–979.

16 (*a*) E. Zhao, J. W. Y. Lam, L. Meng, Y. Hong, H. Deng, G. Bai, X. Huang, J. Hao and B. Z. Tang, *Macromolecules*, 2015, **48**, 64–71; (*b*) W. C. Kim and D. C. Lee, *Polym. Eng. Sci.*, 1995, **35**, 1600–1604.

17 R. B. Restani, P. I. Morgado, M. P. Ribeiro, I. J. Correia, A. A. Ricardo and V. D. B. Bonifacio, *Angew. Chem., Int. Ed.*, 2012, **51**, 5162–5165.

18 Y. Lin, J. W. Gao, H. W. Liu and Y. S. Li, *Macromolecules*, 2009, **42**, 3237–3246.

19 (*a*) D. Wang, Z. Q. Yu, C. Y. Hong and Y. Z. You, *Eur. Polym. J.*, 2013, **49**, 4189–4197; (*b*) Y. Z. You, Z. Q. Yu, M. M. Cui and C. Y. Hong, *Angew. Chem., Int. Ed.*, 2010, **49**, 1099–1102.

20 M. Sun, C. Y. Hong and C. Y. Pan, *J. Am. Chem. Soc.*, 2012, **134**, 20581–19584.

21 Y. Liu and H. S. Goh, *Macromolecules*, 2005, **38**, 9906–9909.

22 D. Wang and T. Imae, *J. Am. Chem. Soc.*, 2004, **126**, 13204–13205.

23 M. R. Eftink, T. J. Selva and Z. Wasylewski, *Photochem. Photobiol.*, 1987, **46**, 23–30.

24 A. Pucci, R. Rausa and F. Ciaredlli, *Macromol. Chem. Phys.*, 2008, **209**, 900–906.

25 C. C. Wang, Z. X. Guo, S. K. Fu, W. Wu and D. B. Zhu, *Prog. Polym. Sci.*, 2004, **29**, 1079–1141.

26 S. W. Kuo and F. C. Chang, *Prog. Polym. Sci.*, 2011, **36**, 1649–1696.

27 A. Fina, O. Monticelli and G. Gamino, *J. Mater. Chem.*, 2010, **20**, 9297–9305.

28 K. W. Huang, L. W. Tsai and S. W. Kuo, *Polymer*, 2009, **50**, 4876–4887.

29 (*a*) Y. Li, H. Su, X. Feng, Z. Wang, K. Guo, C. Wesdemioitis, Q. Fu, S. Z. D. Cheng and W. B. Zhang, *Polym. Chem.*, 2014, **5**, 6151–6162; (*b*) M. Huang, C. H. Hsu, J. Wang, S. Mei, X. Dong, Y. Li, M. Li, H. Liu, W. Zhang, T. Aida, W. B. Zhang, K. Yue and S. Z. D. Cheng, *Science*, 2015, **348**, 424–428; (*c*) Y. Li, H. Su, X. Fneg, K. Yue, Z. Wang, Z. Lin, X. Zhu, Q. Fu, Z. B. Zhang, S. Z. D. Cheng and W. B. Zhang, *Polym. Chem.*, 2015, **6**, 827–837.

30 C. F. Huang, S. W. Kuo, F. J. Lin, W. J. Huang, C. F. Wang, W. Y. Chen and F. C. Chang, *Macromolecules*, 2006, **39**, 300–308.

31 R. Y. Kannan, H. J. Salacinski, P. E. Butler and A. M. Seifalian, *Acc. Chem. Res.*, 2005, **38**, 879–884.

32 D. B. Cordes, P. D. Lickiss and F. Rataboul, *Chem. Rev.*, 2010, **110**, 2081–2173.

33 M. D. Disney, J. Zheng, T. M. Swager and P. H. Seeberger, *J. Am. Chem. Soc.*, 2004, **126**, 13343–13346.

34 B. A. Griffin, S. R. Adams and R. Y. Tsien, *Science*, 1998, **281**, 269–272.

35 J. Wu and P. T. Mather, *Polym. Rev.*, 2009, **49**, 25–63.

36 Y. Tada, H. Yoshida, Y. Ishida, T. Hirai, J. K. Bosworth, E. Dobisz, R. Ruiz, M. Takenaka, T. Hayakawa and H. Hasegawa, *Macromolecules*, 2012, **45**, 9347–9356.

37 T. Hirai, M. Leolukman, T. Hayakawa, M. Kakimoto and P. Gopalan, *Macromolecules*, 2008, **41**, 4558–4560.

38 Y. Ishida, T. Hirai, R. Goseki, M. Tokita, M. A. Kakimoto and T. Hayakawa, *J. Polym. Sci., Part A: Polym. Chem.*, 2011, **49**, 2653–2664.

39 E. S. Cozza, V. Bruzzo, F. Carniato, E. Marsano and O. Monticelli, *ACS Appl. Mater. Interfaces*, 2012, **4**, 604–607.

40 Z. Zhang, L. Hong, Y. Gao and W. Zhang, *Polym. Chem.*, 2014, **5**, 4534–4541.

41 Z. Zhang, L. Hong, J. Li, F. Liu, H. Cai, Y. Gao and W. Zhang, *RSC Adv.*, 2015, **5**, 21580–21587.

42 (*a*) Y. Syuan and S. W. Kuo, *RSC Adv.*, 2014, **4**, 34849–34859; (*b*) Y. J. Yen, S. W. Kuo, C. F. Huang, J. K. Chen and F. C. Chang, *J. Phys. Chem. B*, 2008, **112**, 10821–10829; (*c*) S. W. Kuo, H. C. Lin, W. J. Huang, C. F. Huang and F. C. Chang, *J. Polym. Sci., Part B: Polym. Phys.*, 2006, **44**, 673–686.

43 Y. H. Zhang, J. Huang and Y. M. Chen, *Macromolecules*, 2005, **38**, 5069–5077.

44 J. Z. Du and Y. M. Chen, *Macromolecules*, 2004, **37**, 6322–6328.

45 S. W. Kuo and C. J. Chen, *Macromolecules*, 2012, **45**, 2442–2452.

46 P. O. Danis and E. D. Karr, *Org. Mass Spectrom.*, 1993, **28**, 923–925.

47 L. R. Hutchings, P. P. Brooks, D. Parker, J. A. Mosely and S. Sevinc, *Macromolecules*, 2015, **48**, 610–628.

48 D. C. Schriemer and L. Li, *Anal. Chem.*, 1996, **68**, 2721–2725.

49 (*a*) L. Cui, J. P. Collet, G. Xu and L. Zhu, *Chem. Mater.*, 2006, **18**, 3503–3512; (*b*) Y. J. Sheng, W. J. Lin and W. C. Chen, *J. Chem. Phys.*, 2004, **121**, 9693–9701.

50 (*a*) Y. C. Sheen, C. H. Lu, C. F. Huang, S. W. Kuo and F. C. Chang, *Polymer*, 2008, **49**, 4017–4024; (*b*) A. J. Waddon and E. B. Coughlin, *Chem. Mater.*, 2003, **15**, 4555–4561.

51 R. Ding, Y. Hu, Z. Gui, R. Zong, Z. Chen and W. Fan, *Polym. Degrad. Stab.*, 2003, **81**, 473–476.

52 M. Suzuki and C. A. Wilkie, *Polym. Degrad. Stab.*, 1995, **47**, 217–221.

53 J. J. Yan, Z. K. Wang, X. S. Lin, C. Y. Hong, H. J. Liang, C. Y. Pan and Y. Z. You, *Adv. Mater.*, 2012, **24**, 5617–5624.

54 G. M. Mohamed, H. F. Lu, J. L. Hong and S. W. Kuo, *Polym. Chem.*, 2015, **8**, 6340–6350.